IEEE Access
Multidisciplinary | Rapid Review | Open Access Journal

Received August 27, 2021, accepted September 19, 2021, date of publication September 20, 2021,
date of current version October 5, 2021.

Digital Object Identifier 10.1109/ACCESS.2021.3114356

Rotor Active Magnetic Bearings System Control via a Tuned Nonlinear Saturation Oscillator

ALI KANDIL[1], Y. S. HAMED[2], AND ABDULLAH M. ALSHARIF[2]
[1]Department of Physics and Engineering Mathematics, Faculty of Electronic Engineering, Menoufia University, Menouf 32952, Egypt
[2]Department of Mathematics and Statistics, College of Science, Taif University, Taif 21944, Saudi Arabia

Corresponding author: Ali Kandil (alikandil21@el-eng.menofia.edu.eg)

This work was supported by Taif University Researchers Supporting Project, Taif University, Taif, Saudi Arabia, under Project TURSP-2020/96.

ABSTRACT The proposed work focuses on improving the performance of the traditional nonlinear saturation controller (NSC) algorithm. In this work, a tuning mechanism can be implemented by providing the NSC control unit with the measured speed Ω of the rotor from a shaft encoder device in order to introduce a tuned NSC (TNSC). In other words, we are going to tune the NSC's natural frequency ω_c at one half of Ω such that $\Omega = 2\omega_c$. This TNSC is adopted to reduce the vibratory amplitudes of a 16-pole constant-stiffness rotor-Active magnetic bearings AMBs) system for a wide range of speeds and eccentricities. The whole controlled system is studied mathematically to seek its approximate solutions via the multiple scales technique. Different relations between the rotor's amplitudes and its parameters are plotted so as to verify the proposed tuning mechanism and its crucial role in improving the NSC's performance.

INDEX TERMS Tuned nonlinear saturation controller, proportional derivative controller, active magnetic bearings, shaft encoder, multiple scales technique.

I. INTRODUCTION

Active vibration control is an aim for many researchers around the world. Several mechanical structures and frames may be harmed or even destroyed if they are subjected to mechanical resonance leading to high amplitude vibrations. In this way, the vibrations are actively controlled (relying on feedback signals) such that the unwanted vibrations are suppressed efficiently. Saturation control is one of the approached schemes by scientists to transfer the primary system's unwanted energy to the secondary controller. This is to avoid harming or destroying the expensive mechanical models. Ashour and Nayfeh [1] examined the efficiency of the saturation phenomenon to suppress the vibrations of 2D flexible structures. They developed an adaptive control strategy via a frequency-tuning mechanism where the $2:1$ internal resonance was fulfilled. Felix *et al.* [2] proposed analytical and numerical results of the saturation control of a simple flexible shear-building portal plane frame foundation excited by an unbalanced rotating machine (non-ideal system). Hegazy [3] studied the nonlinear oscillations and saturation phenomena in a hinged-hinged flexible beam. The equation of motion was derived to describe a single-degree-of-freedom system having quadratic damping, cubic and quintic nonlinearities, parametric and external excitations. Jun *et al.* [4] explored the energy transfer mechanism from the excited system to the controller. They examined reducing the large -amplitude vibration of a self-excited system via a nonlinear saturation-based control strategy. Warminski *et al.* [5] studied the effectiveness of several control algorithms in order to suppress the large vibrations of a flexible composite beam. Macro fiber composite (MFC) actuators were involved for implementing the control strategies so as to achieve the required vibration level. They concluded that the best control algorithm used was the nonlinear saturation controller (NSC). Kamel *et al.* [6] applied the NSC to mitigate the unwanted vibrations of a magnetically-levitated body. They derived the frequency response equations via the multiple scales method in order to describe the steady-state behavior of the controlled system. Hamed and Amer [7] studied various types of control algorithms for reducing the large-amplitude vibrations of a flexible composite beam. The effects of different parameters were investigated on the overall behavior of the studied system. Eissa *et al.* [8] considered the time delay effects on the NSC applied to a modified magnetic-levitation model. This time-delayed NSC was quadratically coupled to the main system, then the time delays effects on the system behavior and stability were studied. Kandil and El-Gohary [9],

The associate editor coordinating the review of this manuscript and approving it for publication was Yingxiang Liu.

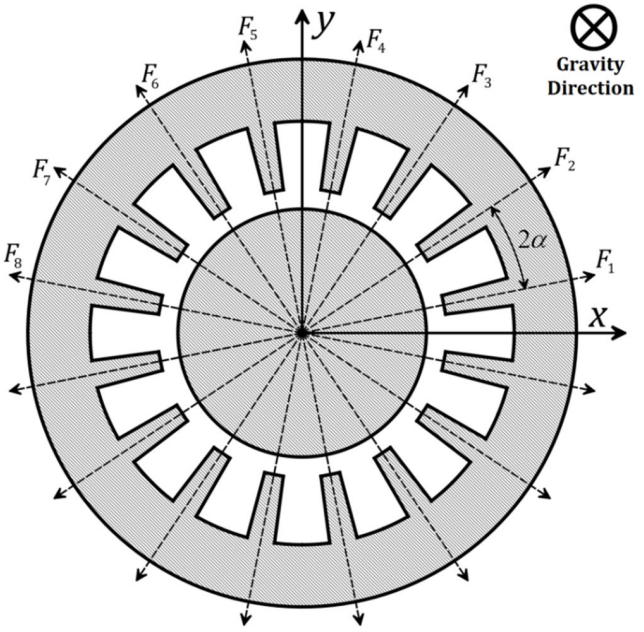

FIGURE 1. Vertical suspension of a rotor between 16 electromagnetic poles.

Hamed and Kandil [10] applied the NSC to the first mode only of a thin-walled rotating beam due to the strong coupling between the first and second modes. They adopted the multiple scales method for extracting the steady-state equations so as to describe the system behavior under the action of NSC. They also considered the effects of time delay on the equilibrium response of the applied NSC.

In this work, our case study model to be controlled is the rotor-active magnetic bearings (AMBs) model which is of a great attention for many physicists and mathematicians. This model may suffer from unwanted vibrations due to the high spinning speed and/or the eccentricity of the rotor. Ji and Hansen [11] concluded that the nonlinearities existence in an AMB model was due to the force-displacement-current characteristics of the electromagnets. Ji [12] investigated the time delays influence on the stability of equilibrium behavior of the rotor-AMBs system. The time delay critical length was determined as a border between stable and unstable motions of the rotor. Zhang and Zhan [13] studied the nonlinear oscillations and chaotic motions in a rotor-AMBs system whose stiffness was time-varying in a periodic form. They considered the rotor's weight which led to that the initial control current was not zero anymore. Inoue *et al.* [14] considered the rigid rotor system supported vertically AMBs, and investigated the time delay effects of both the electric and the magnetic parts of the AMBs on the dynamical characteristics. Yang *et al.* [15] proved that the in-unison and elliptic modal motions were located, and considered the free vibrations of the rotor suspending in the AMBs. Wu *et al.* [16] showed a great consistency between the solutions of the rotor-AMBs original equations and the approximate equations presented by the method of multiple scales. They investigated the complicated nonlinear dynamics

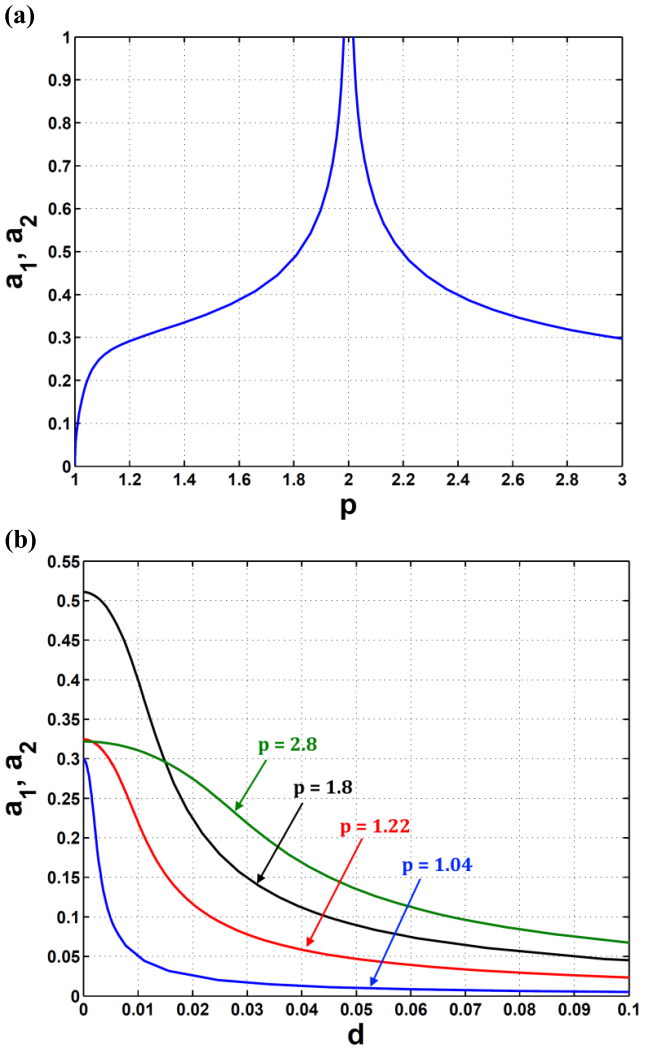

FIGURE 2. The relations between the rotor's oscillation amplitudes a_1 & a_2 and the parameters: (a) p, (b) d, at $\sigma = 0$ and $\lambda = 0$.

near resonances of a rotor-AMB system with 16-pole legs and a time varying stiffness. Jha and Dasgupta [17] proposed an active control scheme through a linearized AMB in order to inhibit the Sommerfeld effect of an internally damped flexible shaft with an eccentric disk mounted at the mid-span. Sun *et al.* [18] discussed a case of an actual AMB system where a typical linear system model and classical linear control theory were utilized in the controller design procedure. Fang *et al.* [19] explored the nonlinear response of the oil-lubricated journal bearing with worn regions analyzed by a wear model. Saeed and Kandil [20], Kandil *et al.* [21], Kandil [22], Saeed and Kandil [23], and Kandil and Hamed [24] investigated the vibrations control of several rotor-AMBs models with different control strategies. The effects of the physical parameters on the solutions stability and multiplicity have been studied and clarified. They presented some recommendations about the rotor's safe behavior in terms of its spinning speed and eccentricity. Ma *et al.* [25] extended the global perturbation technique in order to study the stability and the Shilnikov type multi-pulse

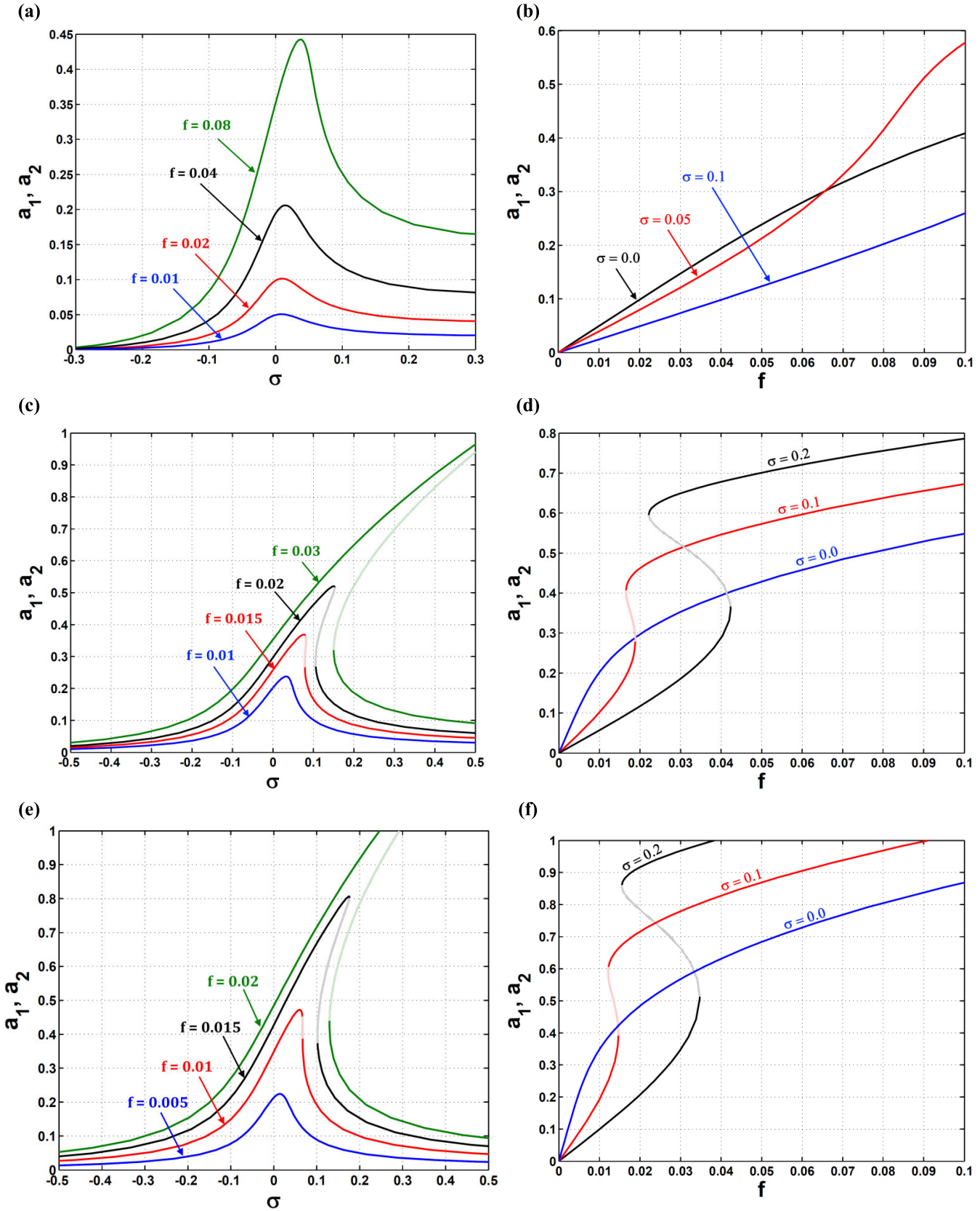

FIGURE 3. The relations between the rotor's oscillation amplitudes a_1 &a_2 and the rotor's speed Ω or eccentricity f at $\lambda = 0$ and: (a, b) $p = 1.04$, (c, d) $p = 1.22$, (e, f) $p = 1.8$, (g, h) $p = 2.8$.

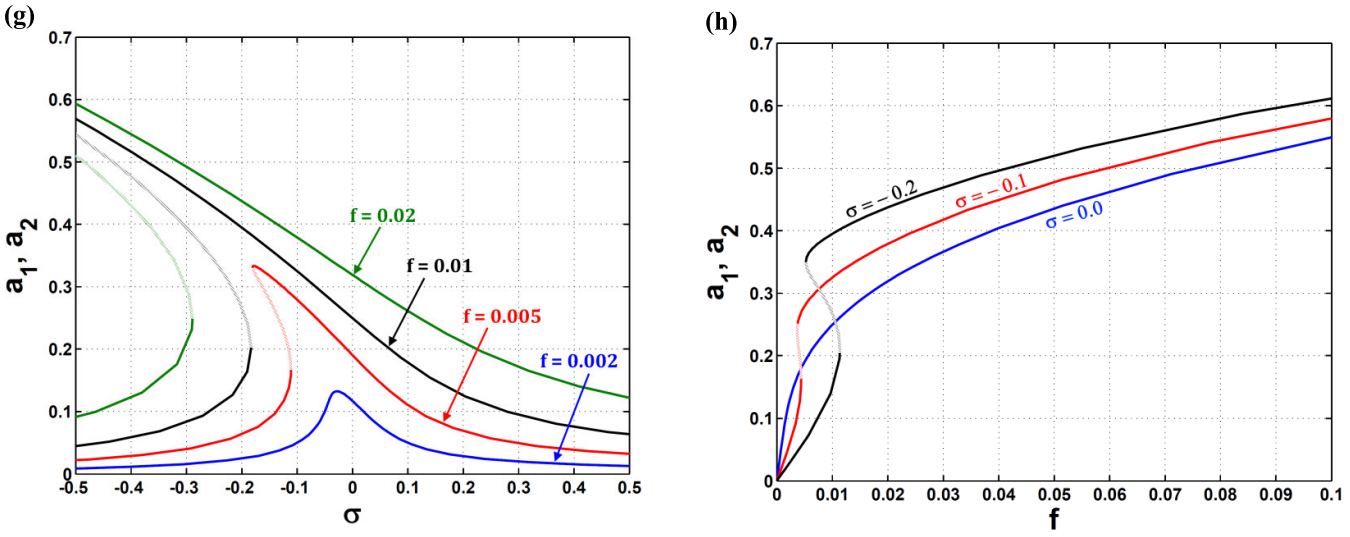

FIGURE 3. *(Continued.)* **The relations between the rotor's oscillation amplitudes a_1 &a_2 and the rotor's speed Ω or eccentricity f at λ = 0 and: (a, b) $p = 1.04$, (c, d) $p = 1.22$, (e, f) $p = 1.8$, (g, h) $p = 2.8$.**

jumping chaotic vibrations in a rotor-AMBs model with a time varying stiffness and 16-pole legs under mechanical and electric-electromagnetic excitations. The contribution of this work is to improve the performance of the conventional NSC control scheme. A tuning mechanism is implemented by providing the NSC control unit with the measured speed Ω of the rotor from a shaft encoder device in order to introduce a TNSC control scheme. This TNSC is adopted to reduce the vibratory amplitudes of a 16-pole constant-stiffness rotor-AMBs model for several values of the rotor's speeds and eccentricities. The multiple scales technique has been utilized to extract the whole controlled system's approximate solutions. Different relations between the rotor's amplitudes and its parameters are plotted so as to verify the proposed tuning mechanism and its crucial role in improving the NSC's performance.

II. MATHEMATICAL ANALYSIS OF THE ROTOR-AMBS DYNAMICS

In this study, the rotor is considered as a rigid non-elastic uniform body which is suspended vertically between the 16 electromagnetic poles separated by an angle $2\alpha = \pi/8$ as shown in Fig. 1. The rotor's Cartesian oscillatory behavior is governed by the following motion equations:

$$m_r\ddot{x} + \zeta_r\dot{x} - R_x = m_r e_r \Omega^2 \cos(\Omega t) \tag{1a}$$
$$m_r\ddot{y} + \zeta_r\dot{y} - R_y = m_r e_r \Omega^2 \sin(\Omega t) \tag{1b}$$

where m_r is the rotor's mass, e_r is its eccentricity, Ω is its angular speed, and ζ_r is a presumed small viscosity parameter. R_x and R_y are the Cartesian resultant electromagnetic restoring forces. Each couple of opposite poles can generate a magnetic force indexed by $n(n = 1, \cdots, 8)$ and can be formulated as [26]:

$$F_n = D\left[\frac{(I_0 - I_n)^2}{(C - z_n)^2} - \frac{(I_0 + I_n)^2}{(C + z_n)^2}\right] \tag{2}$$

where D is a physical constant related to the engineering design of the electromagnets, I_0 is a preliminary magnetization current, I_n is an applied control current on every nth couple of opposite poles, C is an air-gap between the rotor and the poles, z_n is the rotor's radial position due to the nth orientation. Furthermore, the magnetic forces can be controlled by adjusting the current I_n according to the following relation:

$$I_n = k_p z_n + k_d \dot{z}_n - k_1 Z_n \tag{3}$$

where k_p and k_d are known as the PD control gains, k_1 is an extra control gain, Z_n is the additional radial NSC control signal. The functions z_n and Z_n are assumed to be

$$z_n = x\cos((2n-1)\alpha) + y\sin((2n-1)\alpha)$$
$$\Rightarrow \dot{z}_n = \dot{x}\cos((2n-1)\alpha) + \dot{y}\sin((2n-1)\alpha) \tag{4a}$$
$$Z_n = u^2\cos((2n-1)\alpha) + v^2\sin((2n-1)\alpha) \tag{4b}$$

where u and v are known as the NSC control signals that are generated from virtual NSC oscillators of the form

$$\ddot{u} + \zeta_c\dot{u} + \chi_c^2 u = k_2 x u \tag{5a}$$
$$\ddot{v} + \zeta_c\dot{v} + \chi_c^2 v = k_2 y v \tag{5b}$$

where ζ_c is a damping parameter, χ_c is the NSC's natural frequency, k_2 is the feedback gain.

Combining Eqs. (2) to (4) then calculating the resultant Cartesian components magnetic forces to the fourth order as follows

$$\begin{aligned} R_x = {} & \eta_1 k_d\dot{x} + \eta_2 x + \eta_3\left(x^3 + xy^2\right) \\ & + \eta_4 k_d\left(\dot{x}y^2 + 2xy\dot{y} + 3x^2\dot{x}\right) \\ & + \eta_5 k_d^2\left(x\dot{y}^2 + 2\dot{x}y\dot{y} + 3x\dot{x}^2\right) \\ & - \eta_4 k_1\left(u^2y^2 + 2v^2xy + 3u^2x^2\right) \\ & - 2\eta_5 k_1 k_d\left(u^2y\dot{y} + v^2\dot{x}y + v^2x\dot{y} + 3u^2x\dot{x}\right) - \eta_1 k_1 u^2 \end{aligned} \tag{6a}$$

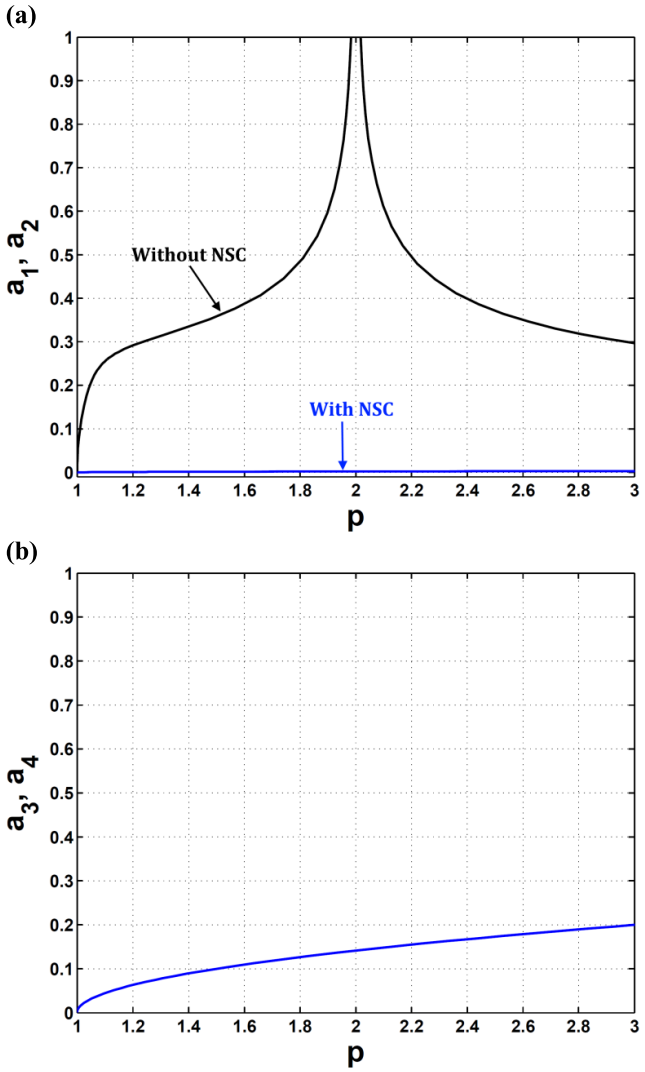

FIGURE 4. The relations between the amplitudes of (a) the rotor, and (b) the controller with the parameter **p** at $\sigma = 0$ and $\lambda = 2$.

$$
\begin{aligned}
R_y = {} & \eta_1 k_d \dot{y} + \eta_2 y + \eta_3 \left(y^3 + x^2 y\right) \\
& + \eta_4 k_d \left(x^2 \dot{y} + 2x\dot{x}y + 3y^2 \dot{y}\right) \\
& + \eta_5 k_d^2 \left(\dot{x}^2 y + 2x\dot{x}\dot{y} + 3y\dot{y}^2\right) \\
& - \eta_4 k_1 \left(v^2 x^2 + 2u^2 xy + 3v^2 y^2\right) \\
& - 2\eta_5 k_1 k_d \left(v^2 x\dot{x} + u^2 x\dot{y} + u^2 \dot{x} y + 3v^2 y\dot{y}\right) - \eta_1 k_1 v^2
\end{aligned} \tag{6b}
$$

where

$$
\eta_1 = -\frac{16DI_0}{C^2} \eta_2 = \frac{16D}{C^3}\left[I_0^2 - k_p C I_0\right]
$$

$$
\eta_3 = \frac{12D}{C^5}\left[2I_0^2 - 3k_p C I_0 + k_p^2 C^2\right] \quad \eta_4 = \frac{4D}{C^4}\left[2k_p C - 3I_0\right]
$$

$$
\eta_5 = \frac{4D}{C^3}
$$

To generalize the rotor's motion coordinates, we can propose that $x = Cx^*$, $y = Cy^*$, $u = Cu^*$, $v = Cv^*$,

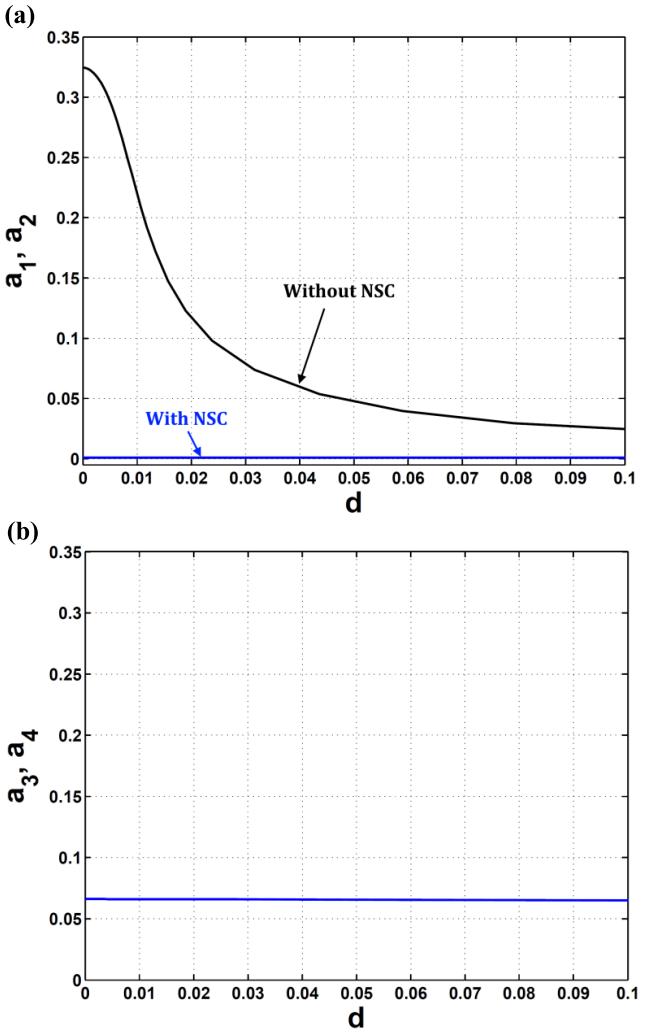

FIGURE 5. The relations between the amplitudes of (a) the rotor, and (b) the controller with the parameter **d** at $\sigma = 0$ and $\lambda = 2$.

$t = t^*\sqrt{m_r C^3 D^{-1} I_0^{-2}}$, $\Omega = \Omega^* t^* t^{-1}$ in order to normalize the coordinates and the time. Hence, inserting Eqs. (6) into (1) with (5) then removing $*$ for simplicity gives us the following:

$$
\begin{aligned}
& \ddot{x} + \mu\dot{x} + \omega^2 x + \alpha_1\left(x^3 + xy^2\right) + \alpha_2\left(\dot{x}y^2 + 2xy\dot{y} + 3x^2\dot{x}\right) \\
& \quad + \alpha_3\left(x\dot{y}^2 + 2\dot{x}y\dot{y} + 3x\dot{x}^2\right) + \beta_1\left(u^2y^2 + 2v^2xy + 3u^2x^2\right) \\
& \quad + \beta_2\left(u^2y\dot{y} + v^2\dot{x}y + v^2x\dot{y} + 3u^2x\dot{x}\right) \\
& = f\Omega^2\cos(\Omega t) + 16\lambda u^2
\end{aligned} \tag{7a}
$$

$$
\begin{aligned}
& \ddot{y} + \mu\dot{y} + \omega^2 y + \alpha_1\left(y^3 + x^2 y\right) \\
& \quad + \alpha_2\left(x^2\dot{y} + 2x\dot{x}y + 3y^2\dot{y}\right) \\
& \quad + \alpha_3\left(\dot{x}^2 y + 2x\dot{x}\dot{y} + 3y\dot{y}^2\right) + \beta_1\left(v^2x^2 + 2u^2xy + 3v^2y^2\right) \\
& \quad + \beta_2\left(v^2x\dot{x} + u^2x\dot{y} + u^2\dot{x}y + 3v^2y\dot{y}\right) \\
& = f\Omega^2\sin(\Omega t) + 16\lambda v^2
\end{aligned} \tag{7b}
$$

$$
\ddot{u} + \mu_c\dot{u} + \omega_c^2 u = \lambda x u \tag{7c}
$$

$$
\ddot{v} + \mu_c\dot{v} + \omega_c^2 v = \lambda y v \tag{7d}
$$

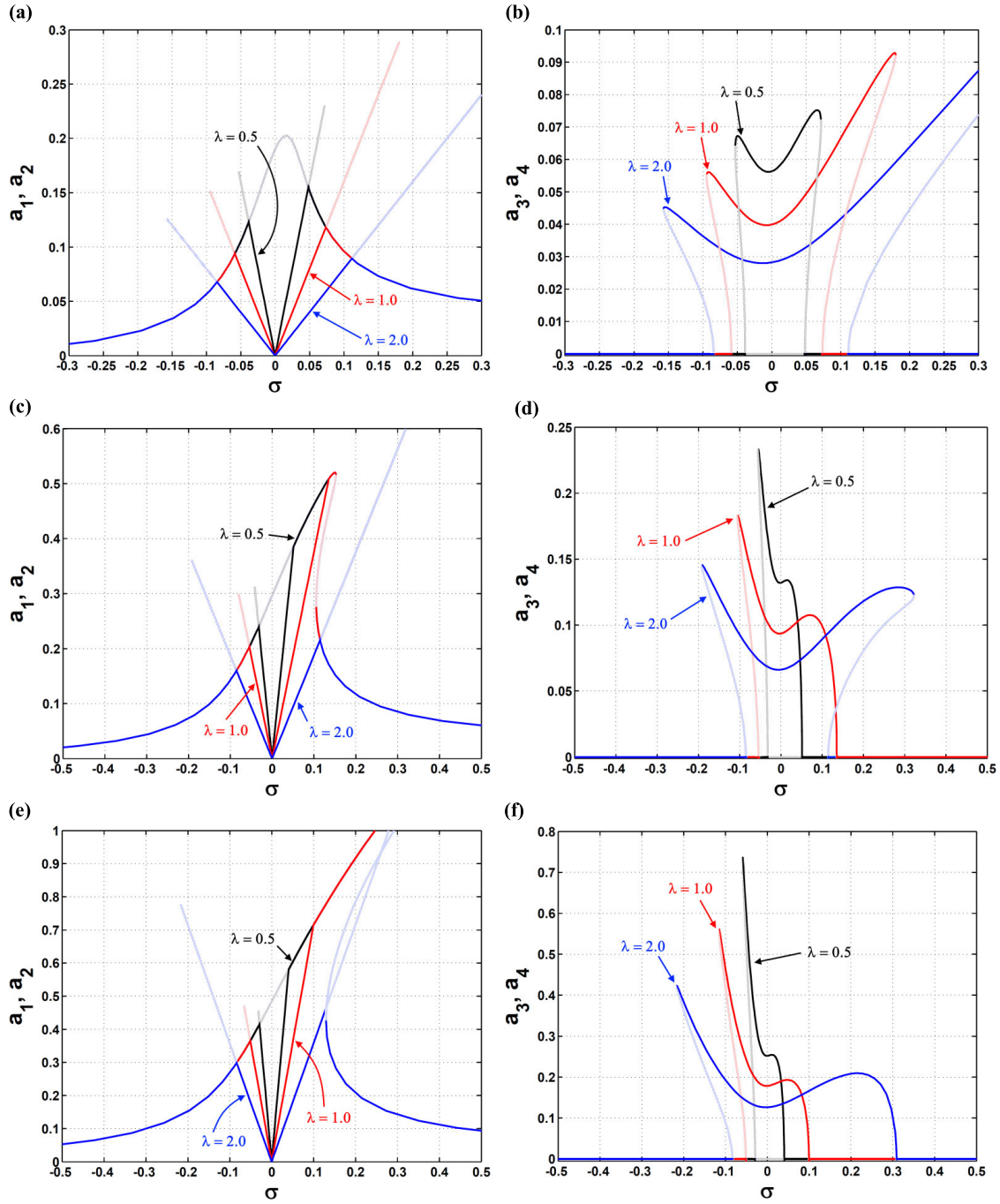

FIGURE 6. The relations between the amplitudes of (*a*, *c*, *e*, *g*) the rotor, and (*b*, *d*, *f*, *b*) the controller, with the parameter σ at distinct λ and: (a, b)$p = 1.04$, (c, d) $p = 1.22$, (e, f) $p = 1.8$, (g, h) $p = 2.8$.

where

$$p = \frac{Ck_p}{I_0} \quad d = \frac{k_d\sqrt{D}}{\sqrt{m_r C}}$$
$$c = \frac{\zeta_r C\sqrt{C}}{I_0\sqrt{m_r D}} \quad f = \frac{e_r}{C}$$
$$\lambda = \frac{C^2 k_1}{I_0} = \frac{k_2 m_r C^4}{DI_0^2} \quad \mu_c = \frac{\zeta_c C\sqrt{m_r C}}{I_0\sqrt{D}}$$
$$\omega_c^2 = \frac{\chi_c^2 m_r C^3}{DI_0^2} \quad \mu = c + 16d$$
$$\omega^2 = 16\,(p-1) \quad \alpha_1 = -12\,(p-1)\,(p-2)$$
$$\alpha_2 = -4d\,(2p-3) \quad \alpha_3 = -4d^2$$
$$\beta_1 = 4\lambda\,(2p-3) \quad \beta_2 = 8\lambda d$$

The system of Eqs. (7) has no exact solution leading us to utilize the multiple scales perturbation technique [27]. In case of $\Omega \approx \omega$ and $2\omega_c \approx \omega$, we can extract approximate solutions of the first order in the form $a_i \cos(\Omega t - \phi_i)$. The modulation on the amplitudes and phases (a_i and ϕ_i) are for the rotor ($i = 1,\ 2$) and the controller ($i = 3,\ 4$) vibrations

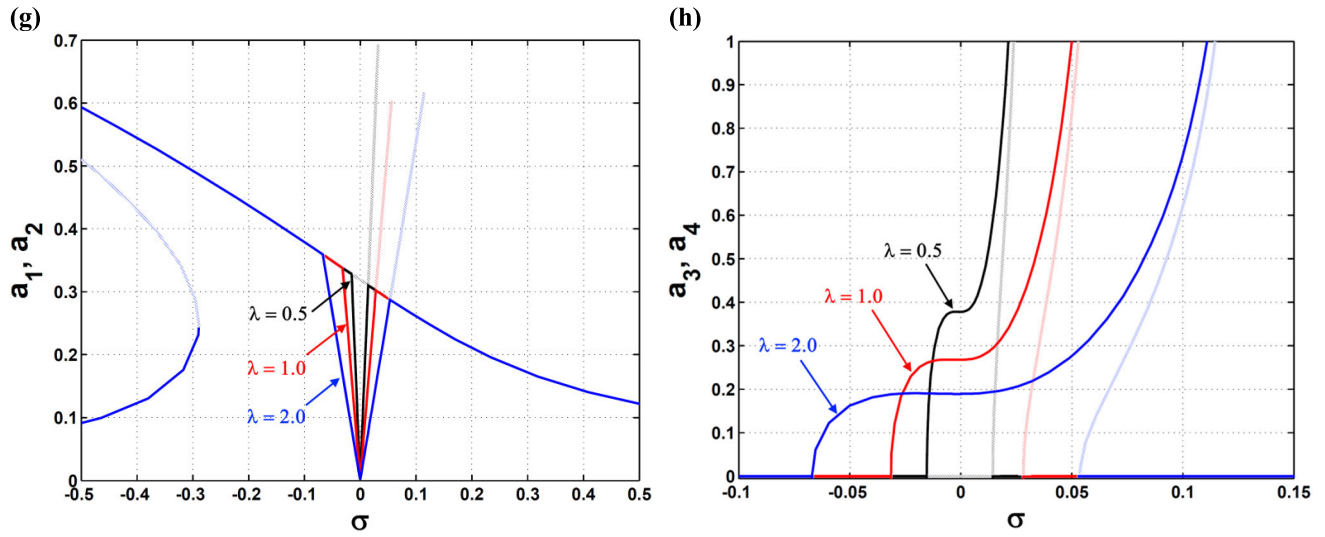

FIGURE 6. *(Continued.)* **The relations between the amplitudes of (*a*, *c*, *e*, *g*) the rotor, and (*b*, *d*, *f*, *b*) the controller, with the parameter σ at distinct λ and: (a, b)$p = 1.04$, (c, d) $p = 1.22$, (e, f) $p = 1.8$, (g, h) $p = 2.8$.**

where they are governed by

$$\begin{aligned}\dot{a}_1 =& -\frac{\mu}{2}a_1 - \frac{\alpha_1+\alpha_3\omega^2}{8\omega}a_1a_2^2\sin(2\phi_1-2\phi_2)\\ &-\frac{\alpha_2}{8}a_1a_2^2\cos(2\phi_1-2\phi_2) - \frac{3\beta_2}{16}a_1^2a_3^2\cos(\phi_1-2\phi_3)\\ &+\left[-\frac{3\beta_1}{16\omega}a_1^2 - \frac{\beta_1}{8\omega}a_2^2 + \frac{4\lambda}{\omega}\right]a_3^2\sin(\phi_1-2\phi_3)\\ &-\frac{\beta_1}{8\omega}a_1a_2a_4^2\sin(2\phi_1-\phi_2-2\phi_4)\\ &-\frac{\beta_1}{16\omega}a_2^2a_3^2\sin(\phi_1-2\phi_2+2\phi_3)\\ &-\frac{\beta_2}{16}a_2^2a_3^2\cos(\phi_1-2\phi_2+2\phi_3)\\ &-\frac{\beta_2}{8}a_1a_2a_4^2\cos(\phi_2-2\phi_4) - \frac{3\alpha_2}{8}a_1^3 - \frac{\alpha_2}{4}a_1a_2^2\\ &+\frac{f\Omega^2}{2\omega}\sin(\phi_1) \qquad (8a)\end{aligned}$$

$$\begin{aligned}\dot{\phi}_1 =& \sigma - \frac{\alpha_1+\alpha_3\omega^2}{8\omega}a_2^2\cos(2\phi_1-2\phi_2)\\ &+\frac{\alpha_2}{8}a_2^2\sin(2\phi_1-2\phi_2) - \frac{3\beta_2}{16}a_1a_3^2\sin(\phi_1-2\phi_3)\\ &+\left[-\frac{9\beta_1}{16\omega}a_1 - \frac{\beta_1}{8\omega}\frac{a_2^2}{a_1} + \frac{4\lambda}{\omega a_1}\right]a_3^2\cos(\phi_1-2\phi_3)\\ &-\frac{\beta_1}{8\omega}a_2a_4^2\cos(2\phi_1-\phi_2-2\phi_4)\\ &-\frac{\beta_1}{16\omega a_1}a_2^2a_3^2\cos(\phi_1-2\phi_2+2\phi_3)\\ &+\frac{\beta_2}{16a_1}a_2^2a_3^2\sin(\phi_1-2\phi_2+2\phi_3)\\ &-\frac{\beta_2}{8}a_2a_4^2\sin(\phi_2-2\phi_4) - \frac{\beta_1}{4\omega}a_2a_4^2\cos(\phi_2-2\phi_4)\\ &-\frac{3\alpha_1+3\alpha_3\omega^2}{8\omega}a_1^2 - \frac{\alpha_1+\alpha_3\omega^2}{4\omega}a_2^2 + \frac{f\Omega^2}{2\omega}\frac{\cos(\phi_1)}{a_1} \qquad (8b)\end{aligned}$$

$$\begin{aligned}\dot{a}_2 =& -\frac{\mu}{2}a_2 + \frac{\alpha_1+\alpha_3\omega^2}{8\omega}a_1^2a_2\sin(2\phi_1-2\phi_2)\\ &-\frac{\alpha_2}{8}a_1^2a_2\cos(2\phi_1-2\phi_2) - \frac{3\beta_2}{16}a_2^2a_4^2\cos(\phi_2-2\phi_4)\\ &+\left[-\frac{3\beta_1}{16\omega}a_2^2 - \frac{\beta_1}{8\omega}a_1^2 + \frac{4\lambda}{\omega}\right]a_4^2\sin(\phi_2-2\phi_4)\\ &+\frac{\beta_1}{8\omega}a_1a_2a_3^2\sin(\phi_1-2\phi_2+2\phi_3)\\ &+\frac{\beta_1}{16\omega}a_1^2a_4^2\sin(2\phi_1-\phi_2-2\phi_4)\\ &-\frac{\beta_2}{16}a_1^2a_4^2\cos(2\phi_1-\phi_2-2\phi_4)\\ &-\frac{\beta_2}{8}a_1a_2a_3^2\cos(\phi_1-2\phi_3) - \frac{3\alpha_2}{8}a_2^3 - \frac{\alpha_2}{4}a_1^2a_2\\ &-\frac{f\Omega^2}{2\omega}\cos(\phi_2) \qquad (8c)\end{aligned}$$

$$\begin{aligned}\dot{\phi}_2 =& \sigma - \frac{\alpha_1+\alpha_3\omega^2}{8\omega}a_1^2\cos(2\phi_1-2\phi_2)\\ &-\frac{\alpha_2}{8}a_1^2\sin(2\phi_1-2\phi_2) - \frac{3\beta_2}{16}a_2a_4^2\sin(\phi_2-2\phi_4)\\ &+\left[-\frac{9\beta_1}{16\omega}a_2 - \frac{\beta_1}{8\omega}\frac{a_1^2}{a_2} + \frac{4\lambda}{\omega a_2}\right]a_4^2\cos(\phi_2-2\phi_4)\\ &-\frac{\beta_1}{8\omega}a_1a_3^2\cos(\phi_1-2\phi_2+2\phi_3)\\ &-\frac{\beta_1}{16\omega a_2}a_1^2a_4^2\cos(2\phi_1-\phi_2-2\phi_4)\\ &-\frac{\beta_2}{16a_2}a_1^2a_4^2\sin(2\phi_1-\phi_2-2\phi_4)\\ &-\frac{\beta_2}{8}a_1a_3^2\sin(\phi_1-2\phi_3) - \frac{\beta_1}{4\omega}a_1a_3^2\cos(\phi_1-2\phi_3)\\ &-\frac{3\alpha_1+3\alpha_3\omega^2}{8\omega}a_2^2 - \frac{\alpha_1+\alpha_3\omega^2}{4\omega}a_1^2 + \frac{f\Omega^2}{2\omega}\frac{\sin(\phi_2)}{a_2} \qquad (8d)\end{aligned}$$

$$\dot{a}_3 = -\frac{\mu_c}{2}a_3 - \frac{\lambda}{4\omega_c}a_1a_3\sin(\phi_1-2\phi_3) \qquad (8e)$$

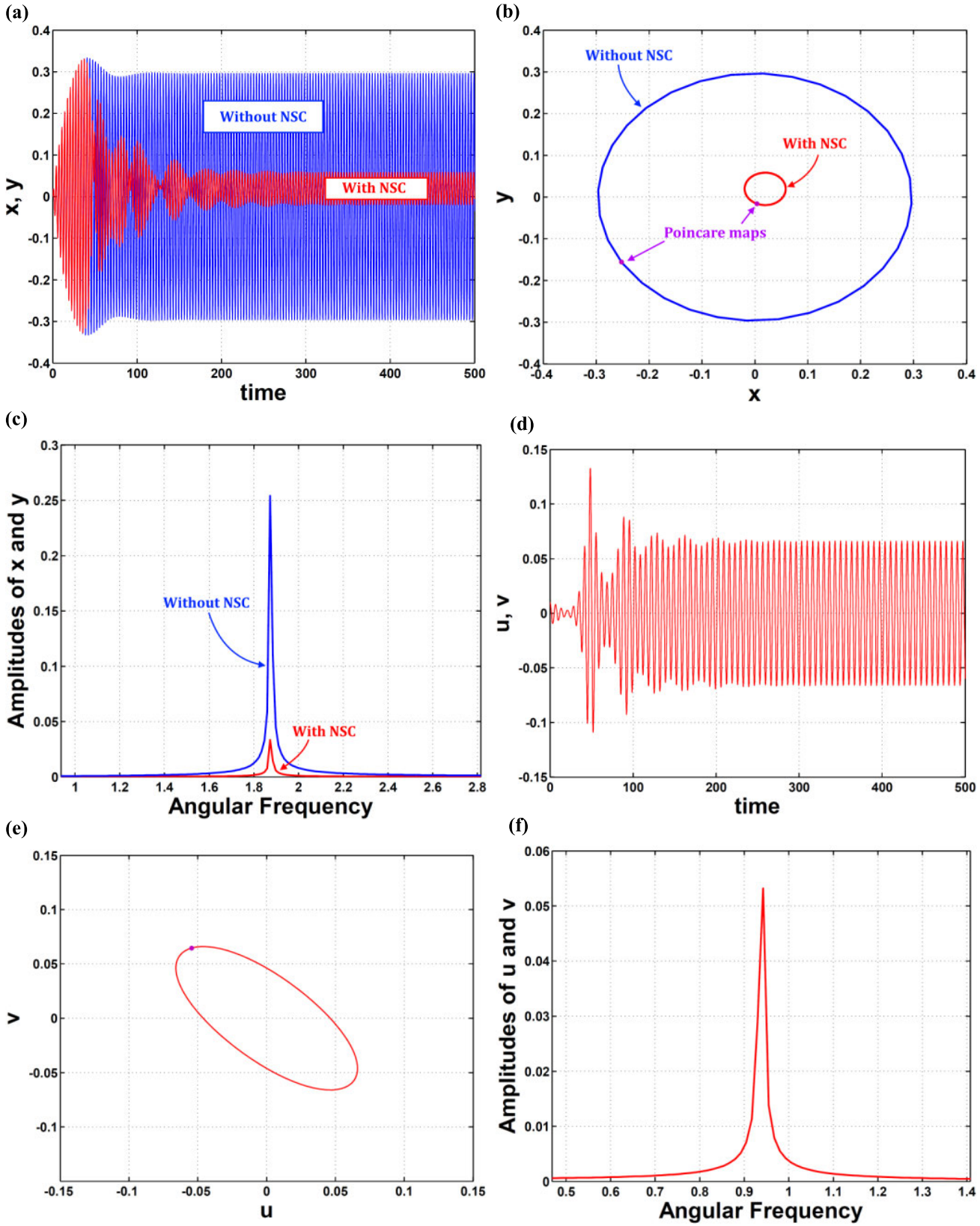

FIGURE 7. The vibratory behavior of (a, b, c) the rotor, and (d, e, f) the controller, represented via (a, d) time responses, (b, e) orbit and Poincare maps, (c, f) frequency spectra at $p = 1.22$, $\sigma = \sigma_c = 0$, $f = 0.02$, and $\lambda = 2.0$.

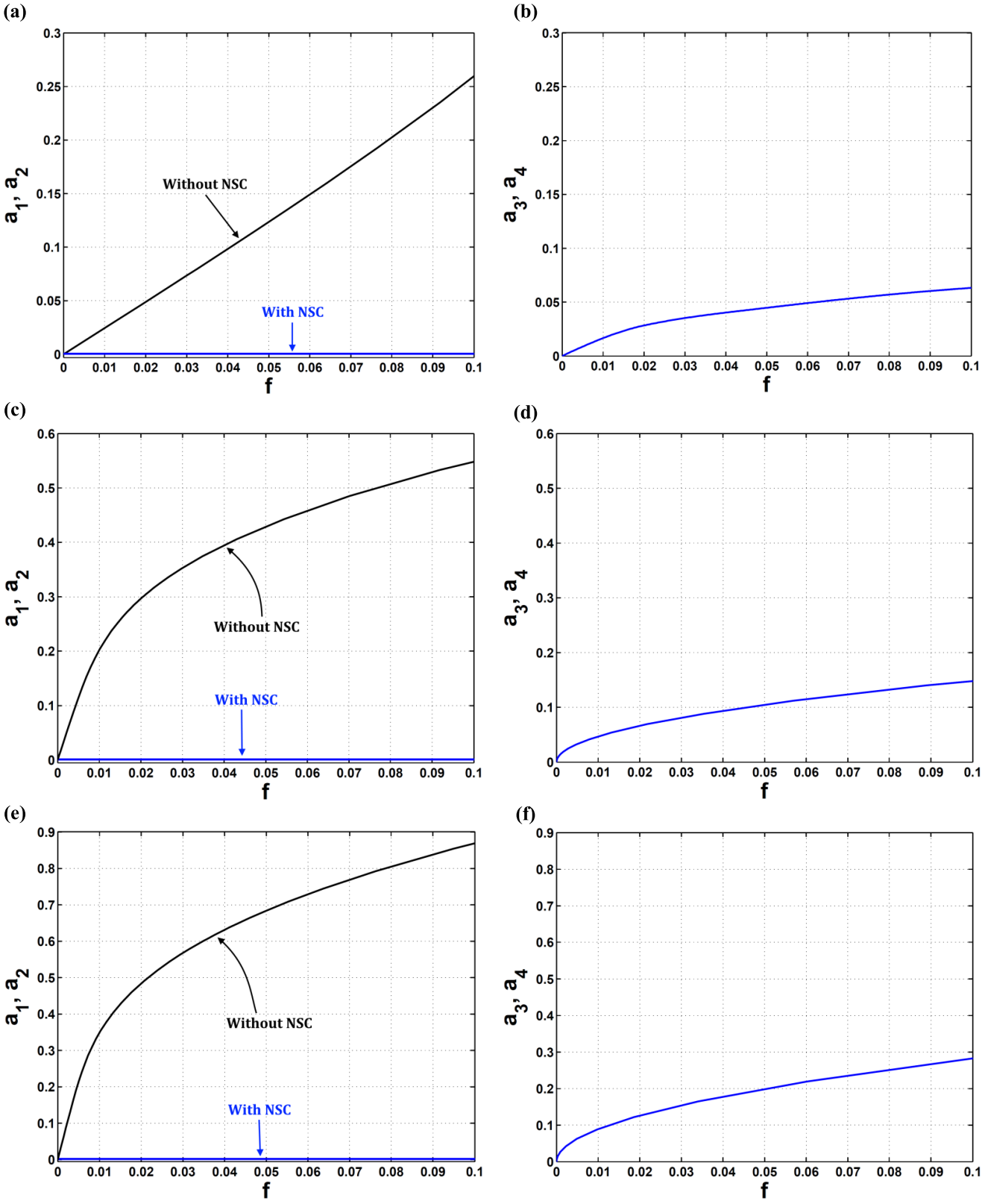

FIGURE 8. The relations between the amplitudes of (a, c, e, g) the rotor, and (b, d, f, h) the NSC controller, with the parameter f at $\sigma = \sigma_c = 0$, $\lambda = 2.0$, and (a, b)$p = 1.04$, (c, d) $p = 1.22$, (e, f) $p = 1.8$, (g, h) $p = 2.8$.

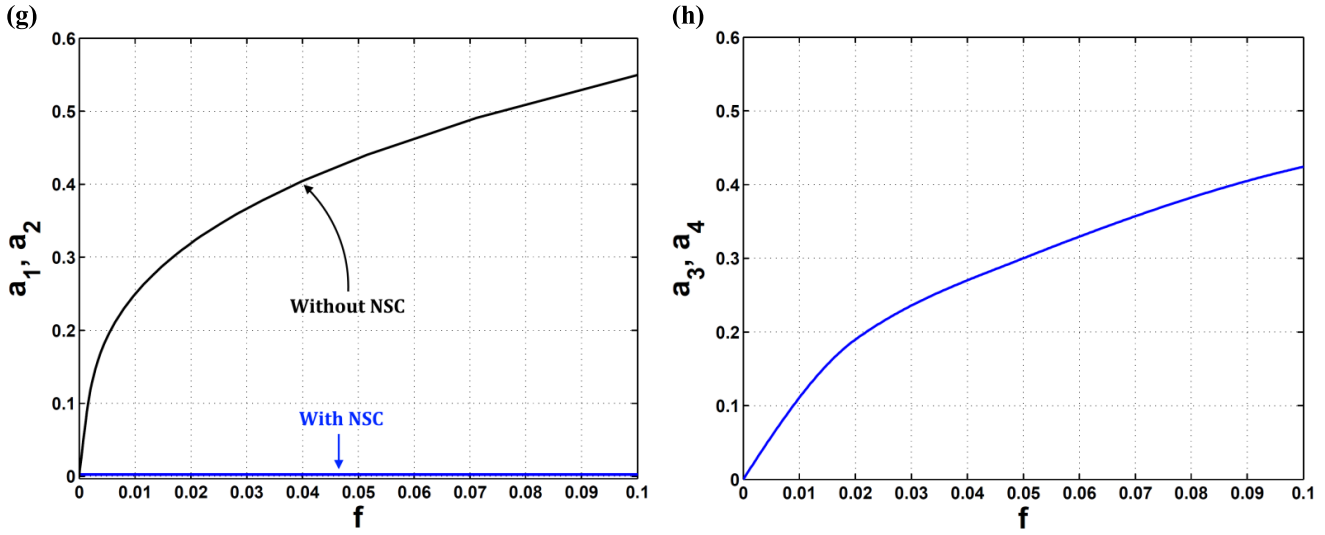

FIGURE 8. *(Continued.)* **The relations between the amplitudes of (a, c, e, g) the rotor, and (b, d, f, h) the NSC controller, with the parameter *f* at $\sigma = \sigma_c = 0$, $\lambda = 2.0$, and (a, b)$p = 1.04$, (c, d) $p = 1.22$, (e, f) $p = 1.8$, (g, h) $p = 2.8$.**

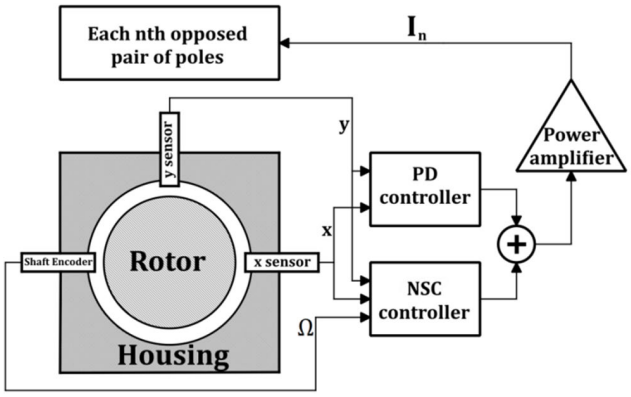

FIGURE 9. **Operation of the TNSC control process.**

$$\dot{\phi}_3 = \sigma - \sigma_c + \frac{\lambda}{4\omega_c} a_1 \cos(\phi_1 - 2\phi_3) \tag{8f}$$

$$\dot{a}_4 = -\frac{\mu_c}{2} a_4 - \frac{\lambda}{4\omega_c} a_2 a_4 \sin(\phi_2 - 2\phi_4) \tag{8g}$$

$$\dot{\phi}_4 = \sigma - \sigma_c + \frac{\lambda}{4\omega_c} a_2 \cos(\phi_2 - 2\phi_4) \tag{8h}$$

where $\sigma = \Omega - \omega$ and $\sigma_c = 2\omega_c - \omega$. Equations (8) have equilibrium points that are found by letting $\dot{a}_i = \dot{\phi}_i = 0$, and they are examined for stability so as to determine whether the point is stable or not according to Hartman-Grobman theorem [28].

III. VIBRATIONAL PERFORMANCE OF THE ROTOR-AMBS IN RESPONSE TO NSC

Here, we are discussing (graphically) the vibrational performance of the rotor-AMBs subjected to the conventional PD controller only (at $\lambda = 0$), both PD and NSC (at $\lambda \neq 0$), both PD and TNSC (at $\lambda \neq 0$). In each case, the changes in different parameters are studied to show the rotor's vibrations dependence on such a change. The optimum parameters' normalized values are the proportional gain $p = 1.04$, the derivative gain $d = 0.005$, the viscosity damping $c = 0.001$, the NSC gain $\lambda = 2.0$, the NSC damping $\mu_c = 0.001$, and the rotor's eccentricity $f = 0.02$, unless otherwise mentioned. It is worthy to remind the reader with that a_1 & a_2 are the rotor's horizontal and vertical oscillation amplitudes, while a_3 & a_4 are the NSC's oscillation amplitudes. In Eqs. (8), the mathematical symmetry can be noticed between a_1 & a_2 and a_3 & a_4 leading us to merge a_1 & a_2 in the same figure and so for a_3 & a_4. The reader should also note that the solid branches refer to stable paths of solutions, but the hatched branches refer to unstable paths of solutions. The rotor's oscillation amplitudes a_1(amplitude of $x^* = x/C$) and a_2(amplitude of $y^* = y/C$) are normalized amplitudes whose original values are always compared to C(the air-gap between the stator and the rotor). Hence, the plotted ranges for a_1 and a_2 should not exceed the value 1 in order to avoid the impact between the stator and the rotor. The adopted parameters above have been chosen based on the same criterion with reasonable values. The relations between the rotor's oscillation amplitudes a_1 & a_2 and the parameters p and d, at $\sigma = 0$ and $\lambda = 0$, are shown in Fig. 2. As been proved in Sec. 2, the rotor's natural frequency $\omega = 4\sqrt{p-1}$ guides us to choose the parameter p value to be > 1 in Fig. 2a, otherwise the system is uncontrollable. In this figure, the amplitudes are directly proportionate to $p \in (1, 2)$. At $p = 2$, the amplitudes become ≥ 1 where the rotor impacts the stator legs. In the range $p > 2$, the operation reverses and the amplitudes are now inversely proportionate to p. It is recommended that p should be chosen away from 2 to avoid the rotor's impact. Furthermore, it is better to approach the lower amplitudes region where $p \to 1$. After several simulation trials, the recommended value of p is 1.04 for a lower amplitude and a controllable rotor operation. Figure 2b

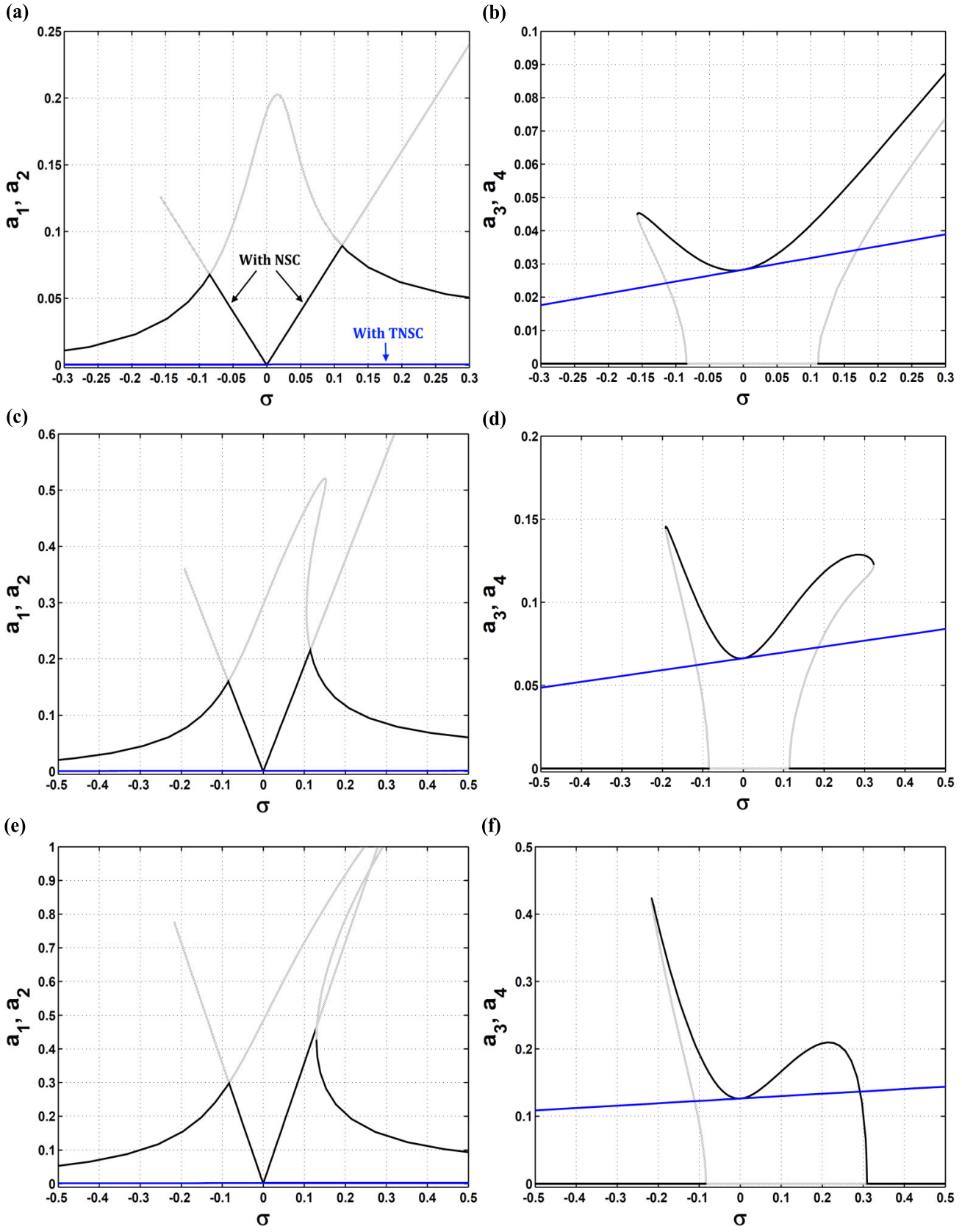

FIGURE 10. The difference between the influences of applying NSC or TNSC on the rotor's speed response curves at $\lambda = 2.0$ and: (a, b) $p = 1.04$, (c, d) $p = 1.22$, (e, f) $p = 1.8$, (g, h) $p = 2.8$.

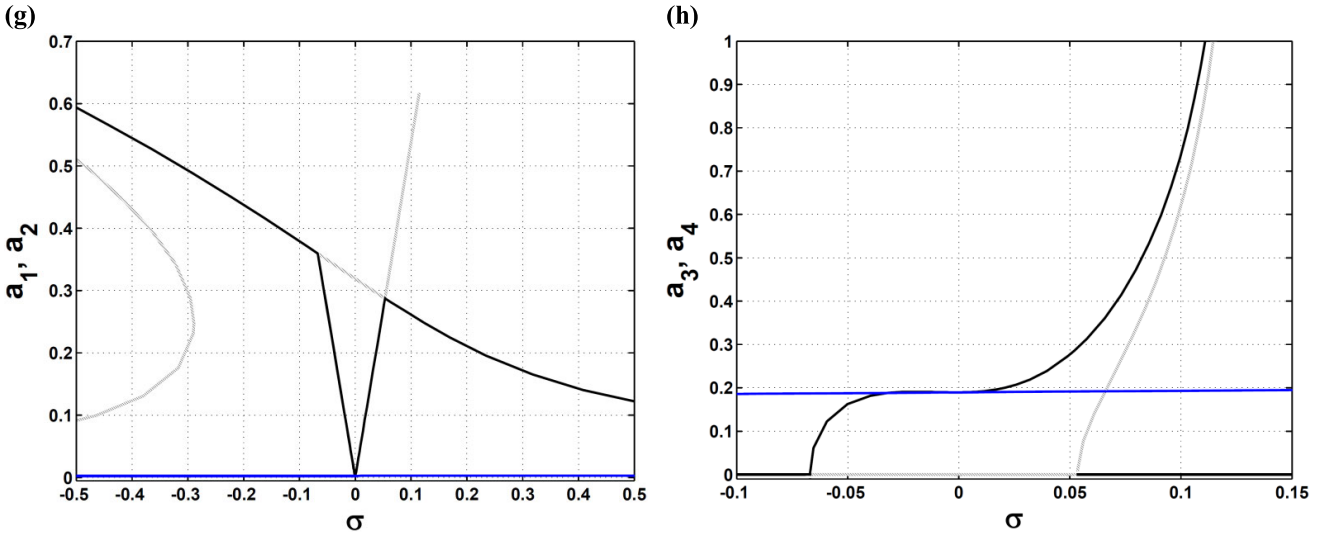

FIGURE 10. *(Contined.)* **The difference between the influences of applying NSC or TNSC on the rotor's speed response curves at $\lambda = 2.0$ and: (a, b) $p = 1.04$, (c, d) $p = 1.22$, (e, f) $p = 1.8$, (g, h) $p = 2.8$.**

clarifies the parameter d improves the amplitudes damping process at different values of p. It is also clear that the smaller the value of p is, the faster the damping process is.

By varying the values of p, we are going to explore the effect of this variation on the relations between the rotor's oscillation amplitudes a_1&a_2 depending on the speed Ω of the rotor ($\sigma = \Omega - \omega$) and its eccentricity f as depicted in Fig. 3. At $p = 1.04$ in Figs. 3a and 3b, the linear behavior is clear for the rotor's amplitudes with respect to Ω and f, respectively. Furthermore at $p = 1.22$ in Figs. 3c and 3d, the curves begin to bend creating jump phenomena between multiple stable paths of solutions and this is due to the domination of the nonlinearities. At $p = 1.8$ in Figs. 3e and 3f, the rotor's vibrations increase where it may impact with the stator ($a_{1,\,2} \geq 1$) at some values of σ and/or f. At $p = 2.8$ in Figs. 3g and 3h, the curves bending changes its direction because α_1 turns negative causing a switch from a hardening case to a softening case. We can see from Figs. 3a and b (at $p = 1.04$) that the rotor has exhibited lower oscillatory amplitudes compared to Figs. 3c to h before applying the NSC. This is a confirmation of Fig. 2.

Next, the application of NSC ($\lambda \neq 0$) is shown to clarify its effect on the relations between the rotor's amplitudes $a_{1,\,2}$ and the parameters p, d, σ and f. Figure 4 shows the difference when the NSC's being OFF ($\lambda = 0$) and ON ($\lambda \neq 0$) according to $p-$ curves at $\sigma = 0$ and $\lambda = 2$. As we can see, the rotor's vibrational amplitudes are saturated at almost zero value regardless of p even if at $p = 2$(where there was a previous impact between the rotor and the stator legs). The same behavior can be seen is in Fig. 5 ($d-$curves) where the rotor's vibrations are saturated at a low level regardless of d.

We should discuss the variation effect of λ on the rotor's vibrations with the application of the NSC controller. Figure 6 illustrates how λ affects the rotor's speed response curves at the different values discussed in Fig. 3. The reader can notice that the NSC has created a V-shape on the old curve for forcing the rotor to follow the new stable path instead of the old path as shown in the figure. The apex of the V-shape is at $\sigma = 0(\Omega = \omega)$ denoting the minimum amplitude approached by the NSC algorithm. Also, one can notice that the apex angle of the V-shape can be adjusted by controlling λ as shown. The higher the parameter λ is, the wider the V-shape is. Another advantage of the V-shape is eliminating the jump phenomena resulted from a change in the rotor's high amplitudes to low amplitudes suddenly and vice versa. A numerical simulation has been achieved on the studied system through MATLAB before and after NSC to confirm our discussion. Figure 7 pictures this simulation as time responses, orbit and Poincare maps, and frequency spectra for both the rotor and the controller at $p = 1.22$, $\sigma = \sigma_c = 0, f = 0.02$, and $\lambda = 2.0$. The given plots show a great influence of using NSC on the rotor's vibrations.

We have discussed the rotor's amplitudes-eccentricity relations when $\sigma = 0$ and $\lambda = 0$(NSC is OFF) at various p as shown before in Fig. 3. On the other hand in Fig. 8, these relations are plotted once more but when $\sigma = \sigma_c = 0$ and $\lambda = 2.0$(NSC is ON) at various p. The influence of using NSC is clear such that the rotor's amplitudes saturate at almost zero value regardless of the change in p. This is due to the saturation phenomenon such that the whole vibrations are transferred from the primary system (the rotor in our case) to the secondary system (the NSC).

To use the benefit of the minimum amplitudes if $\sigma = \sigma_c = 0$, we can guarantee the equality $\sigma = \sigma_c$ not only at 0 but also at wide band of σ values. This mechanism is called tuning mechanism discussed before in Refs. [6, 8-10, 24], or in other words if ω_c is tuned at one half of the rotor speed $\Omega(\Omega = 2\omega_c)$. This can be implemented by providing the NSC control unit with the measured rotor speed Ω from a shaft encoder device shown in Fig. 9. After applying such

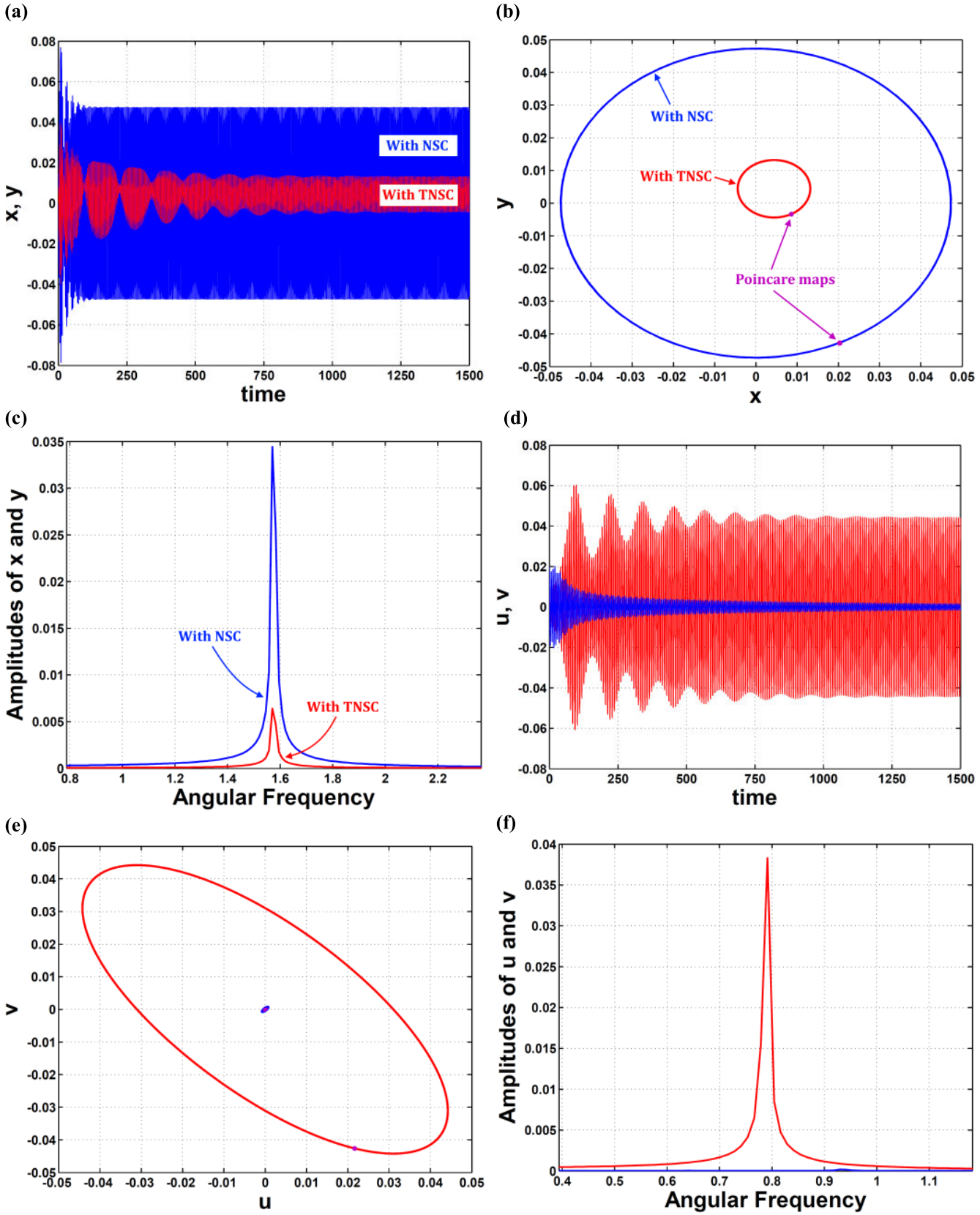

FIGURE 11. The vibratory behavior of (a, b, c) the rotor, and (d, e, f) the controller, represented via (a, d) time responses, (b, e) orbit and Poincare maps, (c, f) frequency spectra at $p = 1.8$, $\sigma = -0.3$, $f = 0.02$, and $\lambda = 2.0$.

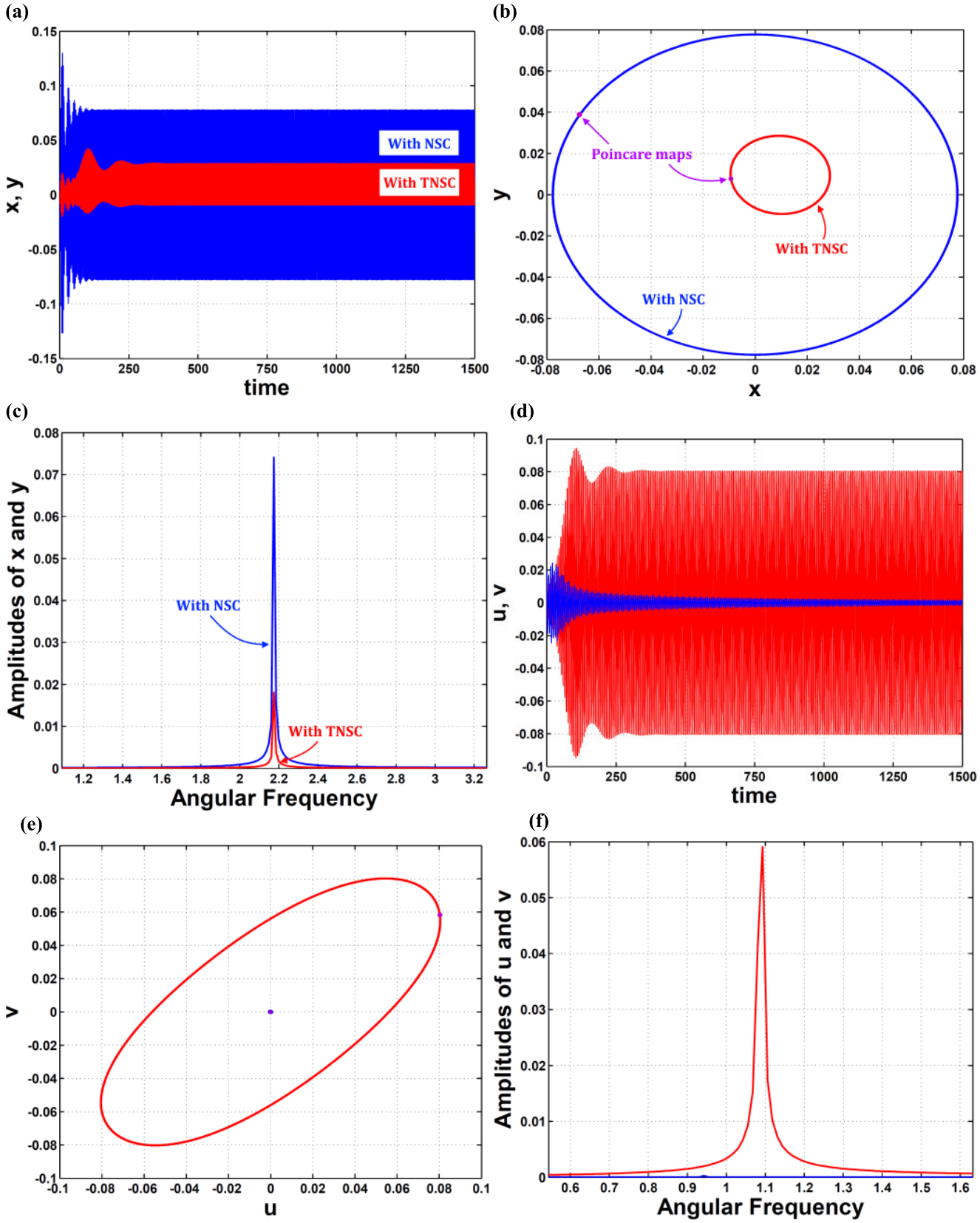

FIGURE 12. The vibratory behavior of (a, b, c) the rotor, and (d, e, f) the controller, represented via (a, d) time responses, (b, e) orbit and Poincare maps, (c, f) frequency spectra at $p = 1.8, \sigma = +0.3, f = 0.02$, and $\lambda = 2.0$.

mechanism ($\Omega = 2\omega_c \Rightarrow \sigma = \sigma_c$), Eqs. (8e) to (8h) will be modified to

$$\dot{a}_3 = -\frac{\mu_c}{2}a_3 - \frac{\lambda}{2\Omega}a_1 a_3 \sin(\phi_1 - 2\phi_3) \tag{9a}$$

$$\dot{\phi}_3 = \frac{\lambda}{2\Omega}a_1 \cos(\phi_1 - 2\phi_3) \tag{9b}$$

$$\dot{a}_4 = -\frac{\mu_c}{2}a_4 - \frac{\lambda}{2\Omega}a_2 a_4 \sin(\phi_2 - 2\phi_4) \tag{9c}$$

$$\dot{\phi}_4 = \frac{\lambda}{2\Omega}a_2 \cos(\phi_2 - 2\phi_4) \tag{9d}$$

At steady state ($\dot{a}_i = \dot{\phi}_i = 0$), simplifying Eqs. (9) with considering $a_3 \neq 0$ and $a_4 \neq 0$ will give us

$$a_1 = a_2 = \frac{\mu_c \Omega}{\lambda} \tag{10}$$

which are the minimum values for both a_1 and a_2. The proposed tuning mechanism leads us to the tuned NSC (TNSC) controller whose influence on the rotor's amplitudes can be observed in comparison with the traditional NSC in Fig. 10. This figure shows the difference between the influences of applying NSC or TNSC on the rotor's speed response curves at $\lambda = 2.0$ and different values of p. Previously in Figs. (6a, c, e, g), we have noticed that the rotor's amplitudes were minima if $\sigma = \sigma_c = 0$ only. Now in Figs. (10a, c, e, g), we see that these amplitudes can be minima for a wide range of σ in case of applying TNSC ($-0.3 \leq (\sigma = \sigma_c) \leq 0.3$) as discussed in Fig. 9. This can also be numerically verified in Figs. 11 and 12 where time responses, orbit and Poincare maps, and frequency spectra are given at $\sigma = -0.3$ and $\sigma = +0.3$, respectively. They assure the great importance of using TNSC rather than NSC.

IV. CONCLUSION

This work was devoted to improve the performance of the traditional NSC control algorithm. A tuning mechanism was achieved by providing the control unit with the rotor's measured speed Ω. All of this was done to propose a modified TNSC control algorithm for reducing the vibratory amplitudes of a 16-poles constant-stiffness rotor-AMBs system. The whole controlled system was studied mathematically to seek its approximate solutions via the multiple scales technique. Different relations between the rotor's amplitudes and its parameters were plotted for discussing our opinion about the topic. Some notes could be summarized as:

- In the absence of NSC ($\lambda = 0$), the rotor's amplitudes were directly proportionate to $p \in (1, 2)$.
- At $p = 2$, the amplitudes became ≥ 1 where the rotor impacted the stator legs. However, the operation reversed and the amplitudes were inversely proportionate to p in the range $p > 2$.
- It was recommended to approach the lower amplitudes region where $p \to 1$, in other words at $p = 1.04$.
- The parameter d improved the damping process at different values of p. This process was faster as p was smaller.
- As p increased, the rotor's speed response curves experienced a change from linear to nonlinear behavior leading to the jump phenomena and unstable paths of solutions.
- In the presence of NSC ($\lambda \neq 0$), the rotor's amplitudes were saturated at almost zero value in the studied ranges of p and d even if at $p = 2$ without impacting the poles.
- A V-shape was imposed on the old curve where the rotor followed the new stable path of solutions instead of the old one as well as eliminating the jump phenomena.
- The apex angle of the V-shape could be adjusted by controlling λ, e.g. the higher the parameter λ was, the wider the V-shape was.
- The NSC made the rotor's amplitudes saturate at almost zero level regardless of the rotor's eccentricity f due to the saturation phenomenon.
- With the discussed tuning mechanism, the rotor's amplitudes became at the lowest levels for a wide range of σ in case of applying the tuned NSC (TNSC).
- For the future work, time delays can be inserted in acquiring the feedback signals and/or applying the control signals in order to approach the real-time procedure.
- Also, the rotor's weight can be included for studying the asymmetry between the rotor's Cartesian oscillations.
- Another future work is stabilizing the whirling motion caused by failure or huge disturbance.

FUNDING

This research received no specific grant from any funding agency in the public, commercial, or not-for-profit sectors.

CONFLICTS OF INTEREST

The authors declared no potential conflicts of interest with respect to the research, authorships, and/or publication of this article.

ACKNOWLEDGMENT

This research was supported by Taif University Researchers Supporting Project Number (TURSP-2020/96), Taif University, Taif, Saudi Arabia.

REFERENCES

[1] O. N. Ashour and A. H. Nayfeh, "Adaptive control of flexible structures using a nonlinear vibration absorber," *Nonlinear Dyn.*, vol. 28, pp. 309–322, Aug. 2002, doi: 10.1023/A:1015622630382.

[2] J. L. P. Felix, J. M. Balthazar, and R. M. L. R. F. Brasil, "On saturation control of a non-ideal vibrating portal frame foundation type shear-building," *J. Vibrat. Control*, vol. 11, no. 1, pp. 121–136, Jan. 2005, doi: 10.1177/1077546305047656.

[3] U. H. Hegazy, "Single-mode response and control of a hinged–hinged flexible beam," *Arch. Appl. Mech.*, vol. 79, no. 4, pp. 335–345, Apr. 2009, doi: 10.1007/s00419-008-0230-9.

[4] L. Jun, L. Xiaobin, and H. Hongxing, "Active nonlinear saturation-based control for suppressing the free vibration of a self-excited plant," *Commun. Nonlinear Sci. Numer. Simul.*, vol. 15, no. 4, pp. 1071–1079, Apr. 2010, doi: 10.1016/j.cnsns.2009.05.028.

[5] J. Warminski, M. Bochenski, W. Jarzyna, P. Filipek, and M. Augustyniak, "Active suppression of nonlinear composite beam vibrations by selected control algorithms," *Commun. Nonlinear Sci. Numer. Simul.*, vol. 16, no. 5, pp. 2237–2248, May 2011, doi: 10.1016/j.cnsns.2010.04.055.

[6] M. Kamel, A. Kandil, W. A. El-Ganaini, and M. Eissa, "Active vibration control of a nonlinear magnetic levitation system via nonlinear saturation controller (NSC)," *Nonlinear Dyn.*, vol. 77, no. 3, pp. 605–619, Aug. 2014, doi: 10.1007/s11071-014-1323-3.
[7] Y. S. Hamed and Y. A. Amer, "Nonlinear saturation controller for vibration supersession of a nonlinear composite beam," *J. Mech. Sci. Technol.*, vol. 28, no. 8, pp. 2987–3002, 2014, doi: 10.1007/s12206-014-0706-1.
[8] M. Eissa, A. Kandil, W. A. El-Ganaini, and M. Kamel, "Vibration suppression of a nonlinear magnetic levitation system via time delayed nonlinear saturation controller," *Int. J. Non-Linear Mech.*, vol. 72, pp. 23–41, Jun. 2015, doi: 10.1016/j.ijnonlinmec.2015.02.012.
[9] A. Kandil and H. A. El-Gohary, "Suppressing the nonlinear vibrations of a compressor blade via a nonlinear saturation controller," *J. Vibrat. Control*, vol. 24, no. 8, pp. 1488–1504, Apr. 2018, doi: 10.1177/1077546316661680.
[10] Y. S. Hamed and A. Kandil, "Influence of time delay on controlling the non-linear oscillations of a rotating blade," *Symmetry*, vol. 13, pp. 1–18, Jan. 2021, doi: 10.3390/sym13010085.
[11] J. C. Ji and C. H. Hansen, "Non-linear oscillations of a rotor in active magnetic bearings," *J. Sound Vibrat.*, vol. 240, no. 4, pp. 599–612, Mar. 2001, doi: 10.1006/jsvi.2000.3257.
[12] J. C. Ji, "Stability and Hopf bifurcation of a magnetic bearing system with time delays," *J. Sound Vib.*, vol. 259, pp. 845–856, Jan. 2003, doi: 10.1006/jsvi.2002.5125.
[13] W. Zhang and X. P. Zhan, "Periodic and chaotic motions of a rotor-active magnetic bearing with quadratic and cubic terms and time-varying stiffness," *Nonlinear Dyn.*, vol. 41, no. 4, pp. 331–359, Sep. 2005, doi: 10.1007/s11071-005-7959-2.
[14] T. Inoue, Y. Sugawara, and M. Sugiyama, "Modeling and nonlinear vibration analysis of a rigid rotor system supported by the magnetic bearing (effects of delays of both electric current and magnetic flux)," *J. Appl. Mech.*, vol. 77, no. 1, pp. 1–10, Jan. 2010, doi: 10.1115/1.3172139.
[15] X.-D. Yang, H.-Z. An, Y.-J. Qian, W. Zhang, and M.-H. Yao, "Elliptic motions and control of rotors suspending in active magnetic bearings," *J. Comput. Nonlinear Dyn.*, vol. 11, no. 5, pp. 1–8, Sep. 2016, doi: 10.1115/1.4033659.
[16] R. Q. Wu, W. Zhang, and M. H. Yao, "Nonlinear dynamics near resonances of a rotor-active magnetic bearings system with 16-pole legs and time varying stiffness," *Mech. Syst. Signal Process.*, vol. 100, pp. 113–134, Feb. 2018, doi: 10.1016/j.ymssp.2017.07.033.
[17] A. K. Jha and S. S. Dasgupta, "Attenuation of Sommerfeld effect in an internally damped eccentric shaft-disk system via active magnetic bearings," *Meccanica*, vol. 54, nos. 1–2, pp. 311–320, Jan. 2019, doi: 10.1007/s11012-018-00936-7.
[18] Z. Sun, X. Zhang, T. Fan, X. Yan, J. Zhao, L. Zhao, and Z. Shi, "Nonlinear dynamic characteristics analysis of active magnetic bearing system based on cell mapping method with a case study," *Mech. Syst. Signal Process.*, vol. 117, pp. 116–137, Feb. 2019, doi: 10.1016/j.ymssp.2018.07.030.
[19] X.-Q. Fang, F.-N. Liu, and S.-P. Yang, "Nonlinear dynamic analysis of worn oil-lubricated rolling bearings," *Proc. Inst. Mech. Eng., E, J. Process Mech. Eng.*, vol. 234, no. 2, pp. 214–221, Apr. 2020, doi: 10.1177/0954408920907541.
[20] N. A. Saeed and A. Kandil, "Lateral vibration control and stabilization of the quasiperiodic oscillations for rotor-active magnetic bearings system," *Nonlinear Dyn.*, vol. 98, no. 2, pp. 1191–1218, Oct. 2019, doi: 10.1007/s11071-019-05256-3.
[21] A. Kandil, M. Sayed, and N. A. Saeed, "On the nonlinear dynamics of constant stiffness coefficients 16-pole rotor active magnetic bearings system," *Eur. J. Mech. A/Solids*, vol. 84, Nov. 2020, Art. no. 104051, doi: 10.1016/j.euromechsol.2020.104051.
[22] A. Kandil, "Investigation of the whirling motion and rub/impact occurrence in a 16-pole rotor active magnetic bearings system with constant stiffness," *Nonlinear Dyn.*, vol. 102, no. 4, pp. 2247–2265, Dec. 2020, doi: 10.1007/s11071-020-06071-x.
[23] N. A. Saeed and A. Kandil, "Two different control strategies for 16-pole rotor active magnetic bearings system with constant stiffness coefficients," *Appl. Math. Model.*, vol. 92, pp. 1–22, Apr. 2021, doi: 10.1016/j.apm.2020.11.005.
[24] A. Kandil and Y. S. Hamed, "Tuned positive position feedback control of an active magnetic bearings system with 16-poles and constant stiffness," *IEEE Access*, vol. 9, pp. 73857–73872, 2021, doi: 10.1109/access.2021.3080457.
[25] W. S. Ma, W. Zhang, and Y. F. Zhang, "Stability and multi-pulse jumping chaotic vibrations of a rotor-active magnetic bearing system with 16-pole legs under mechanical-electric-electromagnetic excitations," *Eur. J. Mech. A/Solids*, vol. 85, Jan. 2021, Art. no. 104120, doi: 10.1016/j.euromechsol.2020.104120.
[26] G. Schweitzer and E. H. *Maslen Magnetic Bearings: Theory, Design, and Application to Rotating Machinery*. Berlin, Germany: Springer, 2009.
[27] A. Nayfeh and D. Mook, *Nonlinear Oscillations*. New York, NY, USA: Wiley, 1995.
[28] A. H. Nayfeh and B. Balachandran, *Applied Nonlinear Dynamics*. New York, NY, USA: Wiley, 1995.

ALI KANDIL received the M.Sc. and Ph.D. degrees in vibration control of nonlinear dynamical systems from the Faculty of Electronic Engineering, Menoufia University, in 2014 and 2018, respectively. He is currently working as an Assistant Professor of engineering mathematics with the Faculty of Electronic Engineering, Menoufia University. His current research interests include vibration control, nonlinear dynamics, bifurcation theory, and stability theory.

Y. S. HAMED received the M.Sc. and Ph.D. degrees in mathematics from the Faculty of Science, Menoufia University, Egypt, in 2005 and 2009, respectively. He is currently a Professor of engineering mathematics with the Department of Physics and Engineering Mathematics, Faculty of Electronic Engineering, Menoufia University. He has been a Professor of mathematics with the Department of Mathematics and Statistics, Taif University, Saudi Arabia. He has supervised and examined some of the M.Sc. and Ph.D. candidates. His research interests include theory of differential equations and its application, numerical analysis, modeling, dynamical systems control, chaotic systems, renewable energy systems, vibration control and computational methods for solving differential equations, and engineering systems. He is an Editor of *International Journal of Control, Automation and Systems* (IJCAS).

ABDULLAH M. ALSHARIF received the Ph.D. degree in mathematics for engineering science from the University of Birmingham, U.K. He has published research articles in reputed international journals of mathematical and engineering sciences. His research interests include applied mathematics and mathematical physics, including the mathematical methods and models for complex systems, Newtonian and non-Newtonian fluids, mathematical engineering, and numerical methods for rheological fluids. He is a referee of mathematical journals.